RSC Advances

ROYAL SOCIETY OF CHEMISTRY

www.rsc.org/advances

Refining nanotopographical features on bone implant surfaces by altering surface chemical compositions

Xiaobing Zhao[a, b], Guocheng Wang[b]†*, Hai Zheng[a], Zufu Lu[b], Xingbao Cheng[a], and Hala Zreiqat[b]*

Graphical abstract

Nb_2O_5/TiO_2 composite coatings with controllable nanostructures by adjusting the amount of Nb_2O_5 were achieved in one simple and single plasma spraying process and Nb_2O_5 doping showed the potential use of TiO_2 coatings in enhancing the biological properties of biomedical coatings.

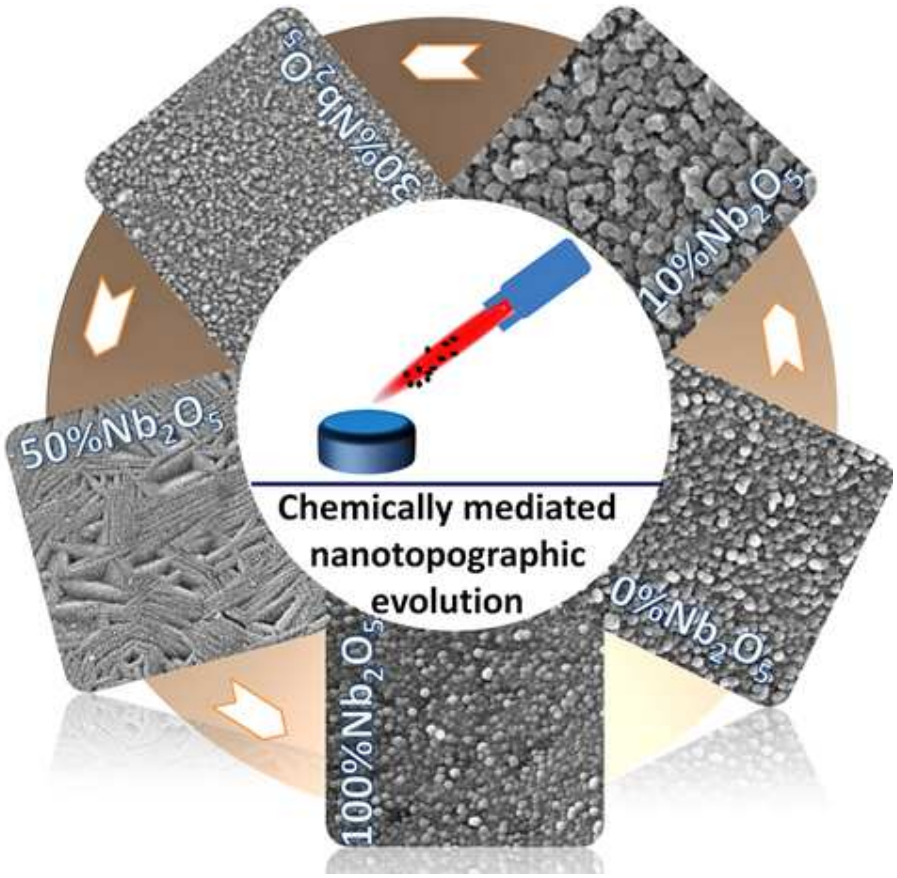

Journal Name

RSCPublishing

ARTICLE

Refining nanotopographical features on bone implant surfaces by altering surface chemical compositions

Cite this: DOI: 10.1039/x0xx00000x

Xiaobing Zhao[a, b], Guocheng Wang[b†*], Hai Zheng[a], Zufu Lu[b], Xingbao Cheng[a], and Hala Zreiqat[b*]

Received 00th January 2012,
Accepted 00th January 2012

DOI: 10.1039/x0xx00000x

www.rsc.org/

Surface nanotopographic and chemical modification are the most often used strategies to improve the performance of the currently used implants due to the well-documented effects of nanotopographic features and surface chemistry on the osseointegration of dental and orthopaedic implants. In this study, a dual-modification of surface chemistry and nanotopography was realized in one single process and a correlation between the surface chemistry and nanotopography was found. We used Nb_2O_5 to change the surface chemical composition of the plasma sprayed TiO_2 coatings, which in turn refined the shapes and sizes of nanotopographic features due to the modulation of the rapid solidification process of plasma spraying. The refinement of nanotopographic features is dose-dependent, and the most prominent effect is found at the 50wt. % Nb_2O_5 doping where a solid solution with a formula of $Ti_{0.95}Nb_{0.95}O_4$ was formed. The introduction of Nb_2O_5 into the TiO_2 matrix also enhanced the corrosion resistance of TiO_2 coatings and improved the bonding strength between the coating and the substrate, which are also dose-dependent. Moreover, it was found that cells on the 50wt. % Nb_2O_5/TiO_2 coating with nanoplate structure showed the highest viability over the culture period. This study demonstrates the potential use of TiO_2 coatings doped with Nb_2O_5 for enhancing the bioactivity of the currently used metallic dental and orthopaedic implants.

1. Introduction

Demand for orthopaedic implants is increasing dramatically, largely due to the growing prevalence of osteoarthritis as the population ages and the road traffic accidents causing a large majority of trauma injuries.[1] Titanium (Ti) and its alloys are extensively used in orthopaedics due to their excellent properties such as low specific weight, high corrosion resistance and good biocompatibility.[2,3] The main problem of Ti implants is their suboptimal surface properties including insufficient bioactivity and corrosion resistance properties.[4,5] Titanium dioxide (TiO_2) has been used as a biomedical coating on Ti and its alloy implants due to its chemical stability, low cost, non-toxicity and biocompatibility [6]. It has been clinically used in applications such as artificial heart valves and vascular stents,[1,7] however, its use in orthopaedic applications is limited due to its poor bioactivity that results in the poor interfacial bonding onto the host bone. To enhance the bioactivity of the TiO_2 coated implants, approaches include changing the surface chemistry and adjusting the topography of the TiO_2 coating have been utilized.

Niobium oxide (Nb_2O_5) as a biomedical material has good corrosion resistance and outstanding biocompatibility.[8] Nb has recently received great attention in the biomedical field either as alloy elements to improve the corrosion resistance of some metal implants or as a second phase for enhancing the biocompatibility of some biomaterials.[9-11] Wang et al.[12] and Zhao et al.[13] demonstrated that Nb modified biomedical metal materials resulted in a metal with improved corrosion resistance and enhanced biocompatibility due to the formation of a Nb_2O_5 layer on the metal surface which prevents metal ion release. We recently incorporated SiO_2 and Nb_2O_5 into plasma sprayed TiO_2 coatings, and compared their individual effects on the bioactivity and electrochemistry properties of the TiO_2 coatings. It was demonstrated that plasma sprayed TiO_2 coatings doped with Nb_2O_5 on the surface of commercially pure Ti implants, had enhanced chemical stability and bioactivity, compared to the pure TiO_2 and the SiO_2 doped TiO_2 coatings, which was ascribed to the changes in the surface chemistry and the generation of special nanoplate network structure formed on the Nb_2O_5/TiO_2 coating.[14] This result implied the potential use of Nb_2O_5 to enhance the bioactivity of the TiO_2 coated implants and also pointed out possibility of refining surface nanotopography by changing the surface chemistry, thus realizing a dual-modification of the implant surface in one single physical process of plasma spraying.

In this study, we try to control the nanotopographical features by adjusting the chemical composition of plasma sprayed TiO_2 coatings and undertake an in-depth investigation of the effects of the Nb_2O_5 dopant on the surface nanotopographies of the TiO_2 coating. To validate the potential application of the Nb_2O_5 doped TiO_2 as a biomedical coating to improve the overall performance of the Ti and its alloy implants, those properties of critical importance for the biomedical application were evaluated including corrosion resistance, bonding strength and bioactivity.

2. Experimental

2.1. Coating fabrication

Commercial TiO_2 (P25, Deggusa) and Nb_2O_5 (Shanghai CNPC powder material Co., Ltd, China) powders were used as feedstocks, with a particle size around 30 nm and 10 μm, respectively. To improve the flowability of the composite powders and to prevent them from agglomeration in the powder feeding process, TiO_2 and Nb_2O_5 powders with weight ratios of 10:0, 9:1, 7:3, 5:5 and 0:10 were thoroughly mixed by ball-milling and reconstituted using the following way: 100g composite powders, 50 mL deionized water and 10 mL poly(vinylalcohol) (PVA) solution (5wt%) were mixed in the ball milling tank for 2 hours, dried at 80 °C for 24 hours and then sieved by 80 mesh sieves. Only powders below 80 meshes were used to deposit the coatings.

An atmospheric plasma spraying (APS) system (9M, Sulzer Metco, USA) was used to produce the coatings on commercially pure titanium (cp-Ti) discs with a dimension of 10 mm×10 mm×1 mm. Prior to plasma spraying, the cp-Ti discs were ultrasonically cleaned in absolute ethanol and grit-blasted with brown corundum. After plasma spraying, the coatings were ultrasonically cleaned in acetone and deionized water. The spraying parameters are listed in Table 1.

Table 1 Spraying parameters of atmospheric plasma spraying

Power (kW)	42
Primary gas pressure (psi)	75
Secondary gas pressure (psi)	50
Primary gas (Ar) flow rate (slpm)	40
Secondary gas (H_2) flow rate (slpm)	12
Spraying distance (mm)	100
Powder feed rate (g/min)	20

2.2. Coating characterization

The phase structures of the plasma sprayed TiO_2, $10\%Nb_2O_5/TiO_2$, $30\%Nb_2O_5/TiO_2$, $50\%Nb_2O_5/TiO_2$ and Nb_2O_5 coatings were examined by X-ray diffraction (XRD) employing a diffractometer of Shimadzu 6000 with Cu Kα radiation (λ=1.5418 Å). Data was obtained from 20-80° (2θ) with a step size of 0.02° at a scanning rate of $4°\cdot min^{-1}$. The surface and cross-sectional morphologies of the coatings were observed by field emission scanning electron microscopy (FESEM, Zeiss Ultra Plus) and scanning electron microscopy (SEM) (Hitachi S3800), respectively. The bonding strength between the coating and the Ti substrate was measured in accordance with ASTM C-633-79 procedure.[15] Four samples were tested independently for statistical analysis.

The surface roughness (Ra) of the coating surfaces was determined by measuring four randomly chosen tracks on each type of coating samples using a surface profilometer (Hommelwerke T8000-C, Germany). Data are presented as mean ± S.D. The corrosion behaviour of the coatings was evaluated by electrochemical workstation (CS400, China) in simulated body fluid (SBF) at 37 °C. A standard three-electrode system was utilized for the electrochemical measurements. The auxiliary and reference electrodes were copper and saturated calomel electrode (SCE), respectively. When the open-circuit potential became almost steady, the coatings with approximate 1 cm^2 exposed to the SBF solution were scanned at a potential sweep rate of $5\ mV\cdot s^{-1}$.

2.3. Cell culture, adhesion and proliferation

Cell culture and cell seeding on the TiO_2, $10\%Nb_2O_5/TiO_2$, $30\%Nb_2O_5/TiO_2$, $50\%Nb_2O_5/TiO_2$ and Nb_2O_5 coatings were performed as previously described.[15-18] Briefly, primary human osteoblasts (HOBs) were first isolated from normal human trabecular bone, with a permission to use discarded human tissue granted by the Human Ethics Committee of the University of Sydney and informed consent was obtained. HOBs were cultured at 37 °C in an atmosphere of 5% CO_2. The medium was refreshed every three days and HOBs at passage 3 were used for the compatibility tests of the developed coatings. 0.5 mL cell suspension with a density of 8.0×10^4 cells per ml was seeded on the coating surface. After culturing for 2 hours, HOBs were fixed in a 4% paraformaldehyde solution. For fluorescence microscopy observation, HOBs cultured on the TiO_2, $10\%Nb_2O_5/TiO_2$, $30\%Nb_2O_5/TiO_2$, $50\%Nb_2O_5/TiO_2$ and Nb_2O_5 coatings were first permeabilized with Triton-X100 (Amresco, USA) for 4 min at room temperature and then stained with rhodamine phalloidin (Invitrogen Detection Technologies, USA) at room temperature for 40 min, followed by rinses with PBS for three times. The cytoskeleton of HOBs was visualized using a Leica TCS SPII Multi-photon Microscope. For SEM observation, HOBs were dehydrated in a series of graded ethanol solution (30, 50, 70, 90, 95, and 100%), and dried in hexamethyldisilizane for 3 min, followed by gold-sputtering prior to SEM observation. A Zeiss Ultra Plus Field Emission scanning electron microscope was used to observe the cell morphology.

AlarmarBlue™ assay (Abd Serotec Ltd., UK) was used to determine HOBs proliferation. Four coating samples were tested for statistical analysis. After 3, 7 and 14 days of culturing, cultured medium was replaced by 1 ml fresh medium with 10% alamarBlue™. After incubation for 5 h, 100 μL culture medium was transferred to a 96-well plate to measure its optical density using an enzyme labeling instrument (MULTISKAN, Thermo Electron Corporation, China) at extinction wavelengths of 570 and 600 nm. The operation of alamarBlue™ assay and calculation of HOBs proliferation was performed strictly according to the user instruction from the company. More details about the proliferation test are detailedly described in our previous work.[19]

2.4. Statistical analysis

For statistical analysis, SPSS 17.0 program was used and the data were expressed as Mean ± S.D. Levene's test was performed to determine the homogeneity of variance for all the data. Tukey HSD post hoc tests were used for the data with homogeneous variance. Tamhane's T2 post hoc was employed in the case that the tested group did not have a homogeneous variance. A p-value of less than 0.05 was considered significant.

3. Results

3.1. Phase composition

Figure 1 shows the XRD patterns of the as-sprayed TiO_2, 10%Nb_2O_5/TiO_2, 30%Nb_2O_5/TiO_2, 50%Nb_2O_5/TiO_2 and Nb_2O_5 coatings. The TiO_2 coating is mainly composed of rutile phase (JCPDS No. 21-1276), while the Nb_2O_5 coating consisted of pseudo-hexagonal phase (JCPDS No.28-0317). The 10%Nb_2O_5/TiO_2 and 30%Nb_2O_5/TiO_2 were composed of rutile phase, indicating that addition of a small amount of Nb_2O_5 into TiO_2 coating (below 30%) did not change the rutile phase structure，despite of the shift of the XRD peaks to low angle due to the intercalation of Nb into the lattice of TiO_2. When the Nb_2O_5 doped amount was up to 50wt%, tetragonal phase $Ti_{0.95}Nb_{0.95}O_4$ (JCPDS 47-0024) solid solution was formed, accompanied by a small amount of anatase phase.

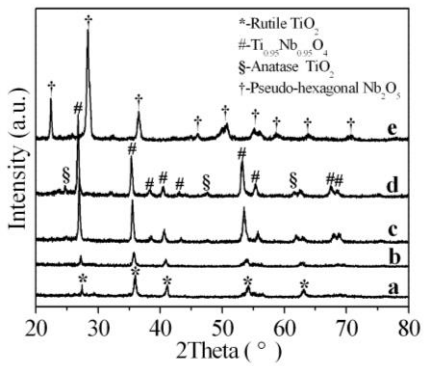

Fig. 1 XRD patterns of the (a) TiO_2, (b) 10%Nb_2O_5/TiO_2, (c) 30%Nb_2O_5/TiO_2, (d) 50%Nb_2O_5 /TiO_2 and (e) Nb_2O_5 coatings.

3.2. Surface and cross-sectional morphology and interfacial bonding

Figure 2 displays the surface morphologies of the TiO_2, 10%Nb_2O_5/TiO_2, 30%Nb_2O_5/TiO_2, 50%Nb_2O_5/TiO_2 and Nb_2O_5 coatings. All coatings exhibit a surface with micro-roughness (Figure 2a), which is one of the typical characteristics of plasma sprayed coatings.[20] Higher magnification images (Figure 2b, c, d, e and f) clearly show that the nanostructures of the TiO_2, 10%Nb_2O_5/TiO_2, 30%Nb_2O_5/TiO_2, 50%Nb_2O_5/TiO_2. The nanostructure of the pure TiO_2 coating was composed of well-defined nanograins with a size around 25 nm (Figure 2b). The TiO_2 coating doped with 10% Nb_2O_5 shared a similar nanostructure to that of the pure TiO_2 coating, however, the nanograins on the surface were stacked forming small aggregates (Figure 2c). For the TiO_2 coating with 30% Nb_2O_5, the grain size in its nanostructure is less-defined and obviously smaller (Figure 2d). The nanostructure of the pure Nb_2O_5 coating resembles that of the pure TiO_2 coating in terms of both the shape and the size of the nanograins (Figure 2f). It is remarkable and interesting that nanoplate network structures (Figure 2e) on 50%Nb_2O_5/TiO_2 coating, which differs from those seen on the other coatings, indicating the great influence imposed by the amount of Nb_2O_5 dopant on the topography of TiO_2 coatings. Figure 3 presents the surface roughness of these five types of coatings. The TiO_2 coating and the Nb_2O_5/TiO_2 composite coatings have similar roughnesses with Ra values between 7 and 10 μm, compared to a much lower surface roughness of the Nb_2O_5 coatings of only 2 μm.

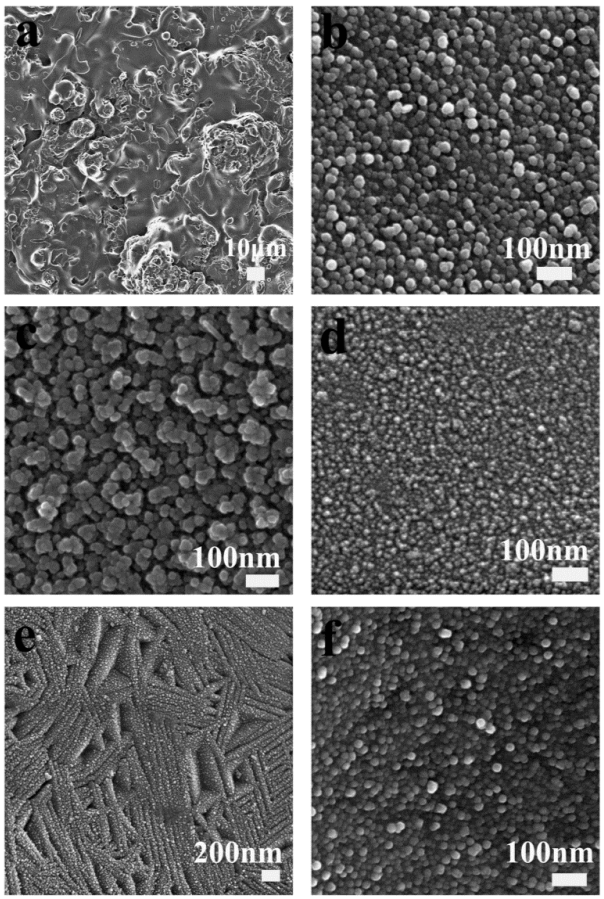

Fig. 2 SEM images of the surface of the TiO_2 coating doped with different percentage of Nb_2O_5: (a) Low magnification image of the pure TiO_2 coating showing the typical rough surface of plasma sprayed coatings; High magnification views of : (b) the pure TiO_2 coating, (c) 10%Nb_2O_5/TiO_2; (d) 30%Nb_2O_5/TiO_2; (e) 50%Nb_2O_5/TiO_2 and (f) Nb_2O_5 coatings.

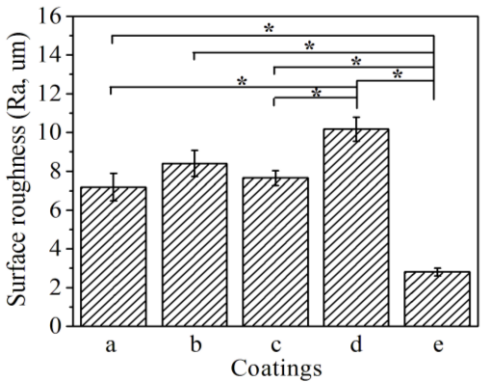

Fig. 3 Surface roughness of the (a) TiO_2, (b) 10%Nb_2O_5/TiO_2, (c) 30%Nb_2O_5/TiO_2, (d) 50%Nb_2O_5 /TiO_2 and (e) Nb_2O_5 coatings, *p<0.05.

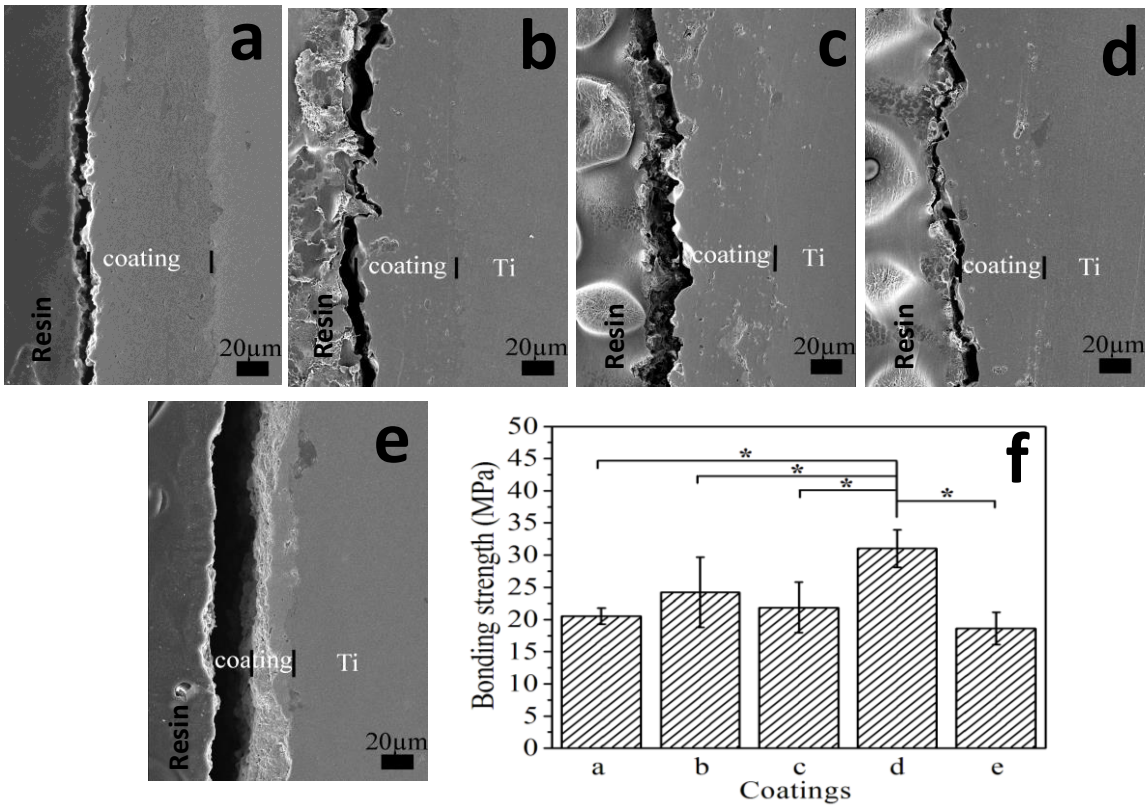

Fig. 4 Cross-sectional images of the (a) TiO_2, (b) 10%Nb_2O_5/TiO_2, (c) 30%Nb_2O_5/TiO_2, (d) 50%Nb_2O_5 /TiO_2, (e) Nb_2O_5 coatings and (f) their bonding strength, *p<0.05.

Figures 4a-e depict the cross-sectional morphologies of the TiO_2, Nb_2O_5 doped TiO_2 and Nb_2O_5 coatings. The TiO_2 coating and the doped TiO_2 coatings have a similar thickness of about 40 μm, but the thickness of Nb_2O_5 coating is only 20 μm, which may be due to the low deposition efficiency of Nb_2O_5 powder driven by its lower density during reconstituted process. The bonding strength of all types of coatings is presented in Figure 4f. The TiO_2, 10%Nb_2O_5/TiO_2, 30%Nb_2O_5/TiO_2 and the Nb_2O_5 coatings have similar bonding strength of around 20 MPa, while the 50%Nb_2O_5/TiO_2 coating displayed the highest bonding strength (31.0 ± 2.9 MPa) among all the types of coatings tested ~~significantly~~.

3.3. Corrosion resistance

Figure 5 presents the potentiodynamic polarization curves of the TiO_2, 10%Nb_2O_5/TiO_2, 30%Nb_2O_5/TiO_2, 50%Nb_2O_5/TiO_2 and Nb_2O_5 coatings tested in SBF solution at 37°C. The corrosion potential (E_{corr}) and corrosion current density (I_{corr}) values of all the coatings are listed in Table 2. The electrode potential is an indicator of corrosion activity; the more negative the potential is, the worse the corrosion resistance will be. The E_{corr} of the Nb_2O_5 coating is -200 mV, much higher than that of the TiO_2 coating (-347 mV), indicating that the Nb_2O_5 coating exhibits better corrosion resistance than that of the TiO_2 coating. The addition of 10% and 50% Nb_2O_5, the corrosion resistance of the TiO_2 coating reflected in the increase in the E_{corr} of the 10% and 50%Nb_2O_5 coatings, compared to that of the TiO_2 coating (Table 2). It is worth noting that the E_{corr} of the 30%Nb_2O_5/TiO_2 coating (-175 mV) is the highest among the five types of coatings tested, suggesting that the addition of 30%Nb_2O_5 in the TiO_2 coating results in a coated surface with the best corrosion resistance. The Nb_2O_5 coating has the lowest I_{corr} value while the TiO_2 coating has the highest, indicating that the TiO_2 coating has the fastest corrosion rate while the Nb_2O_5 coating displaying the slowest corrosion rate. The corrosion rate for the Nb_2O_5 doped TiO_2 coatings falls in between those of TiO_2 and Nb_2O_5 coatings. The 30% Nb_2O_5/TiO_2 coating exhibits the lowest corrosion rate and no significant difference can be found between the other two Nb_2O_5 doped TiO_2 coatings. These results suggest that Nb_2O_5 has a dose-dependent effect on the improvement of the corrosion resistance of the TiO_2 coating.

Table 2 E_{corr} and I_{corr} values determined from the potentiodynamic polarization curves of the coatings obtained in SBF.

Coating	E_{corr} (mV)	I_{corr} (μA/cm^2)
TiO_2	-347	2.25
10%Nb_2O_5/TiO_2	-326	1.57
30%Nb_2O_5/TiO_2	-175	1.05
50%Nb_2O_5/TiO_2	-312	1.56
Nb_2O_5	-200	0.74

3.4. Osteoblast adhesion and proliferation

Figure 6 depicts representative confocal images of HOBs seeded on the surface of the TiO_2, $10\%Nb_2O_5/TiO_2$, $30\%Nb_2O_5/TiO_2$, $50\%Nb_2O_5/TiO_2$ and Nb_2O_5 coatings for 2 hours. After culturing for 2 hours, HOBs flattens on the surfaces of all the coatings. However, fewer HOBs attached to the surface of the $10\%Nb_2O_5/TiO_2$ coating (Figure 6b), compared to those on the surface of the TiO_2, $30\%Nb_2O_5/TiO_2$, $50\%Nb_2O_5/TiO_2$ and Nb_2O_5 coatings (Figure 6a, c, d and e).

Figure 7 depicts SEM images of HOBs cultured for 2 hours on the surface of the TiO_2, $10\%Nb_2O_5/TiO_2$, $30\%Nb_2O_5/TiO_2$, $50\%Nb_2O_5/TiO_2$ and Nb_2O_5 coatings. HOBs cultured on all the types of coatings attach well to the coating surface. Cells cultured on the TiO_2 and the Nb_2O_5 doped TiO_2 coatings (Figure 7a-h) spread out and interact with the coated surfaces, while those on the Nb_2O_5 coatings were less spread.

Figure 8 depicts the proliferation of HOBs on the TiO_2, $10\%Nb_2O_5/TiO_2$, $30\%Nb_2O_5/TiO_2$, $50\%Nb_2O_5/TiO_2$ and Nb_2O_5 coatings. The proliferation rates of HOBs on all coatings increase with the increase in the culture time. In the initial 3 days of culture, the HOB proliferation rate on $50\%Nb_2O_5/TiO_2$ coating is higher than those on the other coatings. After culturing for 7 days, similar proliferation rates was seen for TiO_2, $30\%Nb_2O_5/TiO_2$, $50\%Nb_2O_5/TiO_2$ and Nb_2O_5, which are significantly higher than that of HOBs cultured on the $10\%Nb_2O_5/TiO_2$. At day 14, significantly higher proliferation rate was observed for the HOBs cultured on the $50\%Nb_2O_5/TiO_2$ coating, compared to those cultured on the other coatings.

The *in vitro* bioactivity studies suggest that the addition of 30% and in particular 50% Nb_2O_5 enhances the bioactivity of the TiO_2 coating, whereas the addition of 10% Nb_2O_5 slightly compromises the bioactivity of the TiO_2 coating, indicating that the impact of Nb_2O_5 on the bioactivity of TiO_2 coatings is dependent on its doped amount.

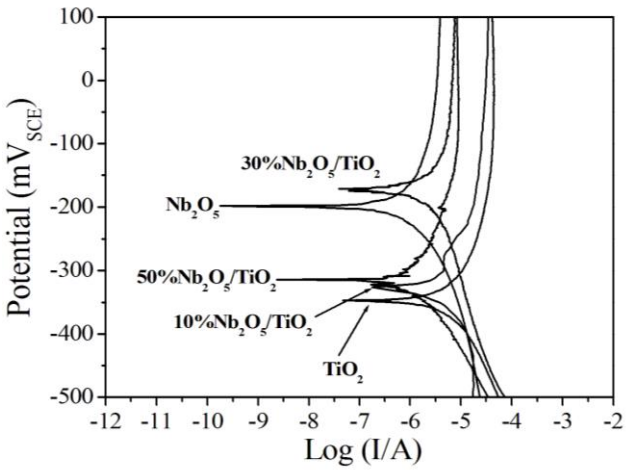

Fig. 5 Potentiodynamic polarization curves of the TiO_2, $10\%Nb_2O_5/TiO_2$, $30\%Nb_2O_5/TiO_2$, $50\%Nb_2O_5/TiO_2$ and Nb_2O_5 coatings.

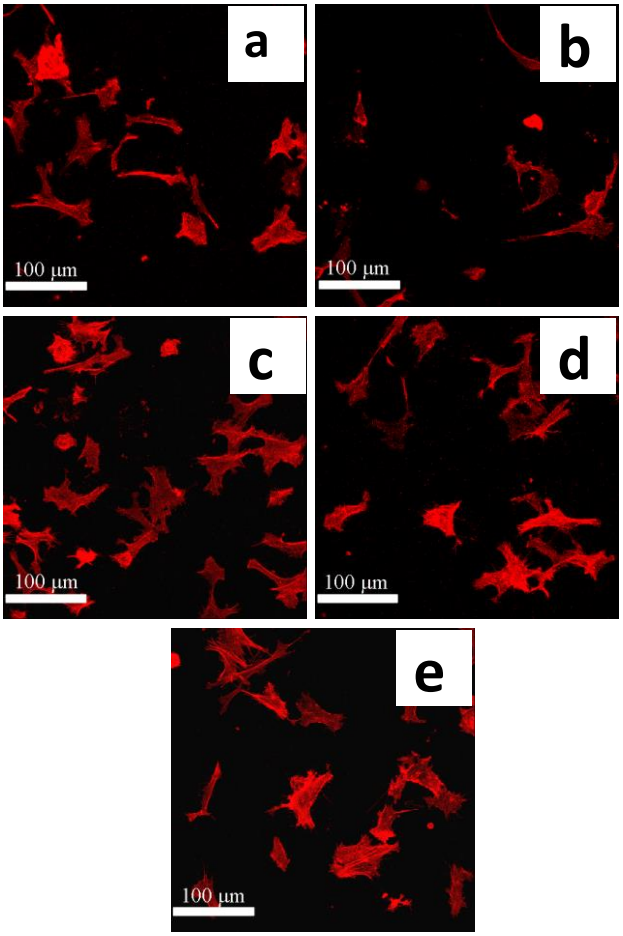

Fig. 6 Confocal images of HOBs seeded for 2 hours on the surface of the (a) TiO_2, (b) $10\%Nb_2O_5/TiO_2$, (c) $30\%Nb_2O_5/TiO_2$, (d) $50\%Nb_2O_5$ /TiO_2 and (e) Nb_2O_5 coatings.

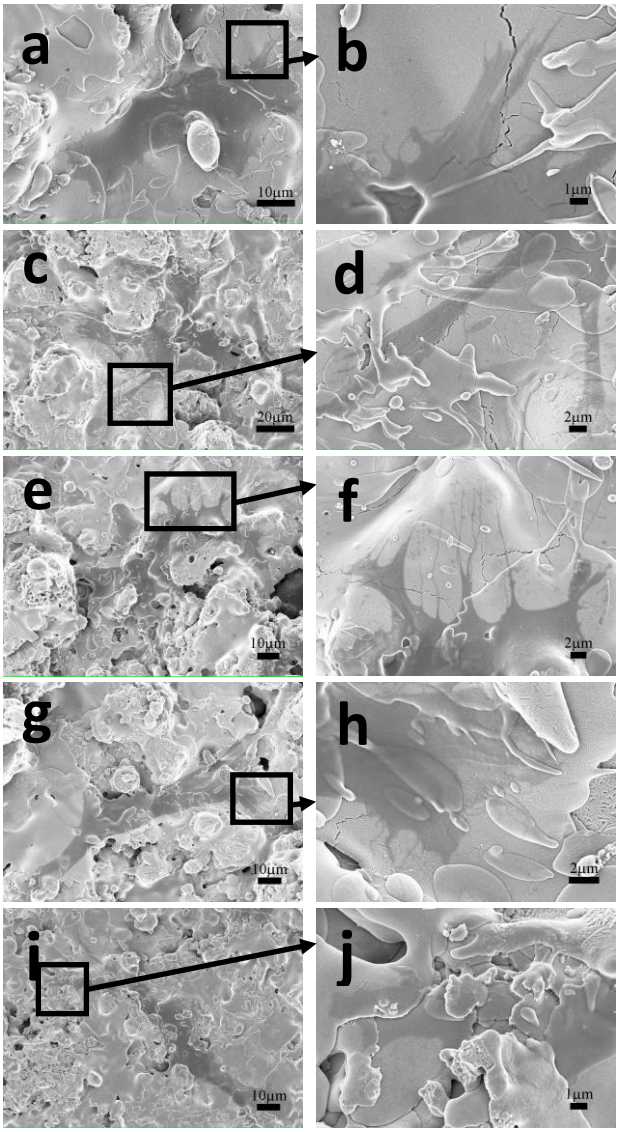

Fig. 7 SEM micrographs of HOBs cultured on the (a, b) TiO_2, (c, d) 10%Nb_2O_5/TiO_2, (e, f) 30%Nb_2O_5/TiO_2, (g, h) 50%Nb_2O_5/TiO_2 and (i, j) Nb_2O_5 coatings (Images (b) (d) (f) (h) and (j) are under higher magnifications).

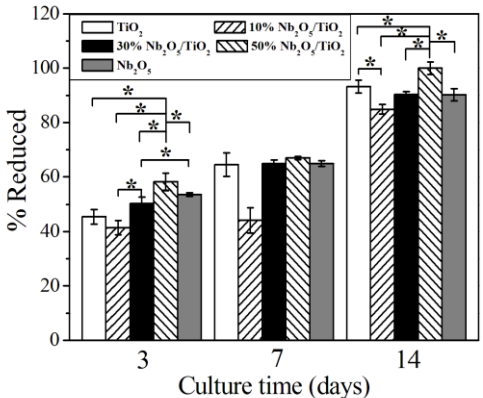

Fig. 8 HOB proliferation on the TiO_2, 10%Nb_2O_5/TiO_2, 30%Nb_2O_5/TiO_2, 50%Nb_2O_5/TiO_2 and Nb_2O_5 coatings after culturing for 3, 7 and 14 days, *p<0.05.

4. Discussion

The surface characteristics of artificial implant materials, such as chemical composition, topography, roughness and hydrophilicity, are critical for the success of the implant.[21-23] In this study, to improve the surface properties of TiO_2 coatings for their better application as biomedical coatings, a chemically stable and biocompatible oxide (Nb_2O_5) [10,13,24] was incorporated into TiO_2 coatings using plasma spraying, which not only improved the corrosion resistance properties, but also enhanced the bioactivity and biocompatibility of the TiO_2 coatings.[14] Importantly, we found that the addition of Nb_2O_5 can refine the nanotopographic features of the TiO_2 coating, thus providing an approach capable of changing surface chemistry and refining surface nanotopography in one simple physical process. As the importance of both surface chemistry and nanotopography on the biological performance of biomedical implants, the findings in our study may provide new insight of innovative application of traditional plasma spaying in future biomedical implant coating design.

Our results demonstrated that small amounts of Nb_2O_5 does not affect the crystalline structures of the TiO_2 coatings as Nb is intercalated into the spaces between TiO_2 octahedron sheets during the coating process (solidification).[25-27] This intercalation resulted in shifting of the TiO_2 peaks to lower angles in the XRD pattern for the Nb_2O_5 doped TiO_2 coatings (Figure 1b and c). In contrast, increase in the doped amount of Nb_2O_5 to 50 wt.% resulted in the formation of a new solid solution phase ($Ti_{0.95}Nb_{0.95}O_4$) and a small amount of anatase phase (Figure 1d) on the TiO_2 coatings (Figure 1d). Since TiO_2 coating exists in the form of rutile phase in the TiO_2 coatings (Figure 1a), the formation of the small amount of anatase phase is possible because Nb doping inhibits phase transformation of TiO_2 from anatase to rutile in the solidification process. This is in agreement with others who demonstrated the inhibition effect of Nb on the anatase-rutile transformation.[27,28] Interestingly, the changes in the crystalline phase are accompanied by the morphological evolution (Figure 2) from nanostructures composed of nanosized spherical grains (the TiO_2, Nb_2O_5, 10 wt.% and 30 wt.% Nb_2O_5/TiO_2 coatings) into nanoplate network structures (the 50% Nb_2O_5/TiO_2 coatings) (Figure 2a-f). The formation of this special nanostructure was supposed to be ascribed to the recrystallization of the molten particles during the rapid solidification process of plasma spraying.[21] Under the unique thermal conditions of plasma spraying (high flame temperature and ultra-rapid cooling rate), the growth of crystallites in the process of recrystallization is strongly suppressed, leading to the formation of the nano-sized grains.[21,29] The formation of this nanostructure, which is based on the rapid solidification under the high cooling rate, is influenced by many factors including the temperature of the substrate, spraying processing parameters (e.g. powers, ratio of H_2/Ar) and the auxiliary cooling conditions.[30] In addition, the thermo-physical property of the spraying material itself is also of great importance to recrystallization process, thus influencing the final size and shape of the nanotopographic features on the surface. Among all the Nb_2O_5/TiO_2 coatings, the most prominent changes in the nanotopography occurred in the TiO_2 coating incorporated by 50% Nb_2O_5, which was thought to be ascribed to the formation of the new solid solution phase which is highly possible to cause the changes in the thermodynamics of the recrystallization process.

The interfacial bonding between the coating and the underlying substrate plays an important role in the long-term stability of the implants and a strong bonding between the implant and the coating is a critical in avoiding coating delamination.[31,32] Among all the five types of coatings tested in this study, the 50%Nb_2O_5/TiO_2 coating

exhibits the highest bonding strength to the underlying substrate (Figure 4f), whereas addition of 10 wt.% and 30 wt.% Nb_2O_5 has no prominent effect on the bonding strength of the TiO_2 coating. Coefficient of thermal expansion (CET) is a critical factor in influencing the quality of the coatings and their interface with the underlying substrates. The CETs of TiO_2, Nb_2O_5 and cp-Ti were reported to be 8.0-10.0×10^{-6}·K^{-1},[33] 5.3-5.9 ×10^{-6}·K^{-1},[34] and 9.7-9.9×10^{-6}·K^{-1},[35] respectively. Due to the mismatch of the CETs between the cp-Ti and Nb_2O_5, the addition of 10% and 30% into the TiO_2 matrix does not affect the bonding strength of the TiO_2 coating (Figure 4f). However, prominent improvement in the interfacial bonding strength is observed when the amount of Nb_2O_5 increases to 50% which is highly possible because of the formation of the new $Ti_{0.95}Nb_{0.95}O_4$ phase. We speculate that $Ti_{0.95}Nb_{0.95}O_4$ phase might have a CET much closer to that of cp-Ti substrate. In-depth investigation into the effect of Nb_2O_5 amount on the CETs of Nb_2O_5/TiO_2 composite coatings will be carried out in our future study to validate this hypothesis.

Corrosion resistance is one of the most important surface properties determining the overall success of an orthopaedic implant; it influences the stability and biosafety of the implants by inhibiting the release of non-compatible metal ions which can cause allergic and toxic reactions.[5,36] This study demonstrated that plasma sprayed Nb_2O_5 coatings have superior corrosion resistance compared to the TiO_2 coatings, reflected in both E_{corr} and I_{corr} values (Figure 5, Table 2). We further confirmed that the addition of Nb_2O_5 into TiO_2 matrix improves the corrosion resistance of the TiO_2 coating in a dose-dependent manner. Compared to the TiO_2 coatings doped with 10% and 50% Nb_2O_5, 30% Nb_2O_5/TiO_2 coatings display better corrosion resistance and lower corrosion rate (Table 2). The corrosion resistance ability of a material is influenced by its physical chemistry properties. It was reported that there is a negative correlation between the pitting potential of the oxide coated metal and the point of zero charge (PZC) of the oxide.[13] A lower PZC indicates a higher pitting potential and better corrosion resistance.[37] The PZC of Nb_2O_5 was reported to be 2.8, much lower than that of TiO_2 (5.2), resulting in a better corrosion resistance of Nb_2O_5 than that of TiO_2.[13,37,38] As the 10% Nb_2O_5/TiO_2 and 30% Nb_2O_5/TiO_2 coatings are composed of TiO_2 and Nb_2O_5 phases, the PZCs of these composite coatings should fall between the PZCs of the TiO_2 and Nb_2O_5. Due to the increased amount of Nb_2O_5, the PZC of the 30%Nb_2O_5/TiO_2 coating is expected to be lower compared to that of the 10%Nb_2O_5/TiO_2 coating, which accounts for the better corrosion resistance of the 30%Nb_2O_5/TiO_2 coating. However, as the doped amount of Nb_2O_5 escalated up to 50%, a new solid solution phase ($Ti_{0.95}Nb_{0.95}O_4$) was formed, which may be the reason for the decline of the corrosion resistance of the 50% Nb_2O_5/TiO_2 coating compared to the 30%Nb_2O_5/TiO_2 coating.

Cell adhesion and proliferation are two important biological reactions of the osteoblast to the underlying substrate surface, which can be greatly influenced by the implant surface properties. The TiO_2 and Nb_2O_5 coatings have comparable biocompatibility (here specific to cellular adhesion and proliferation). In agreement with our previous finding[14] and that of others,[12,13] we demonstrated in this study that the incorporation of Nb_2O_5 into TiO_2 matrix improves the biocompatibility of the TiO_2 coatings, however obvious enhancement effect is only observed when the amount of Nb_2O_5 increases up to 50% (Figure 6, 7 and 8). Although the exact mechanism(s) behind this dose-dependent effect of Nb_2O_5 on the biocompatibility is still unclear, we speculate that the differences in the surface chemistry and topography among these different types of coatings resulted in this dose-dependent effect on the coatings biocompatibility.

Compared to the TiO_2 and the other Nb_2O_5 doped TiO_2 coatings, 50% Nb_2O_5/TiO_2 coatings not only modified the surface chemistry by Nb_2O_5 but also resulted in the introduction of special surface topography. The addition of 50% into TiO_2 matrix changes the surface chemical compositions such that a larger amount of Nb element is exposed on the surface to interact with the seeded osteoblasts. Nb is a biocompatible element and has been recently used to enhance the biocompatibility of biomaterials.[9-13] For example, Ding et al.[39] reported that Nb doped TiO_2 nanotubes displayed an enhanced *in vitro* bioactivity and promoted mesenchymal stem cell adhesion and the formation of extracellular matrix, compared to the untapped TiO_2 nanotubes. Topographically, 50%Nb_2O_5/TiO_2 coating not only possesses increased surface micro-roughness but also have unique surface nanostructure, contributing to its enhanced biocompatibility. Micro-roughness has been reported to increase bone anchorage and reinforce the biomechanical interlocking between the bone and the implant.[40] The effect of nanostructure on cell behaviors has been widely studied and it was revealed that the influence of the nanotopographical features is dependent on their physical status, e.g. shapes and sizes.[41-43] We previously demonstrated that the nanosized rod-shaped hydroxyapatite more efficiently enhanced the cellular activity compared to nanosized spherical hydroxyapatite.[44] In this study, the nanoplate formed on the surface of the 50% Nb_2O_5/TiO_2 coating exhibits a rod-liked shape with a high aspect ratio, which is the predominant topographical difference of the 50% Nb_2O_5 doped coating from the others. Therefore, it is plausible to suggest that the unique nanostructure formed on the 50% Nb_2O_5/TiO_2 coating also accounts largely for the better biocompatibility of the coating.

In summary, in this study, we establish that incorporation of Nb_2O_5 into TiO_2 coatings in a dose-dependent manner improves the corrosion resistance, bonding strength and biocompatibility of the Ti implants. This study indicates the potential application of Nb_2O_5 in improving the long-term performance of Ti-based implants through changes in surface chemistry and surface nanotopography.

5. Conclusions

To improve the biological performance of currently used Ti-based implants and shed light on the potential of Nb_2O_5 for biomedical application, TiO_2 coatings doped with different percents of Nb_2O_5 were deposited on cp-Ti substrates by APS. Coating properties relating to the long-term performance, e.g. corrosion resistance, interfacial bonding strength and biocompatibility were studied in correlation with the Nb_2O_5 dopant amount. The addition of Nb_2O_5 does not change the crystalline structure of the TiO_2 at low amounts (10% and 30%), however, a new solid solution phase is formed when the doped amount of Nb_2O_5 increases to 50%, which is highly possible reason for the formation of the unique nanotopography composed of nanoplate network. Results obtained demonstrated a dose-dependent effect of Nb_2O_5 on the corrosion resistance, biocompatibility and interfacial bonding strength of the TiO_2 coating. The 50% Nb_2O_5 doped TiO_2 coating exhibited the best biocompatibility and the highest bonding strength. However, improvement in the corrosion resistance of the 50% Nb_2O_5 coatings was relatively less predominant than the 30% Nb_2O_5 doped TiO_2 coating. Further study will be carried out to find the best composition ratio of Nb_2O_5 and TiO_2 between 30% and 50%, with which the composite coating possesses the best balanced overall properties.

Acknowledgments

The authors give thanks to Jiangsu Overseas Research & Training Program for University Prominent Young & Middle-aged Teachers and Presidents and Australia National Health and Medical Research Council (NHMRC), Australian Research Council (ARC) and the Rebecca Cooper Foundation. The authors thank Australian Centre for Microscopy & Microanalysis for their assistance in Micro/Nano analysis.

Notes and references

[a]*School of Materials Science and Engineering, Changzhou University, Changzhou 213164, China*
[b]*Biomaterials and Tissue Engineering Research Unit, School of AMME, The University of Sydney, Sydney 2006, Australia*
**Corresponding Authors, Dr. Guocheng Wang (gwang@cicbiomagune.es) and Prof. Hala Zreiqat (hala.zreiqat@sydney.edu.au), Tel: +61 2 9351 2392*
[†]*Present Addresses, PP MIRAMON (CIC BIOMAGUNE) Nº 182, PTA C, 20009, DONOSTIA/S SEBSTIAN, GIPUZKOA, SPAIN; Tel: +34 943005321*

1. M. Geetha, A. K. Singh, R. Asokamani and A. K. Gogia, *Prog. Mater. Sci*., 2009, **54**, 397.
2. X. Zhu, J. Chen, L. Scheideler, R. Reichl and J. Geis-Gerstorfer, *Biomaterials*, 2004, **25**, 4087.
3. M. Long and H. J. Rack, *Biomaterials*, 1998 ,**19**, 162.
4. J. M. Gomez-Vega, E. Saiz and A. P. Tomsia, *J. Biomed. Mater. Res.*,1999, **46**, 549.
5. N. Zaveri, M. Mahapatra, A. Deceuster, Y. Peng, L. Li and A. Zhou, *Electrochim. Acta*, 2008, **53**, 5022.
6. A. Ochsenbein, F. Chai, S. Winter, M. Traisne, J. Breme and H. F. Hildebrand, *Acta Biomater.*, 2008, **4**, 1506.
7. H. Shao, C. Yu, X. Xu, J. Wang, R. Zhai and X. Wang, *Appl. Surf. Sci.*, 2010, **257**, 1649.
8. H. Matsuno, A. Yokoyama, F. Watari, M. Uo and T. Kawasaki, *Biomaterials*, 2001, **22**, 1253.
9. R. L. Karlinsey, A. T. Hara, K. Yi and C. W. Duhn, *Biomed. Mater.*, 2006, **1**, 16.
10. E. Eisenbarth, D. Velten and J. Breme, *Biomol. Eng.*, 2007, **24**, 27.
11. F. Y. Zhou, B. L. Wang, K. J. Qiu, W. J. Lin, L. Li, Y. B. Wang, F. L. Nie and Y. F. Zheng, *Mater. Sci. Eng. C*, 2012, **32**, 851.
12. Y. B. Wang and Y. F. Zheng, *Mater. Lett.*, 2009, **63**, 1293.
13. T. Zhao, Y. Li, Y. Xiang, X. Zhao and T. Zhang, *Surf. Coat. Technol.*, 2011, **205**, 4404.
14. X. Zhao, G. Wang, H. Zheng, Z. Lu, X. Zhong, X. Cheng and H. Zreiqat, *ACS Appl. Mater. Interfaces*, 2013, **5**, 8203.
15. G. Wang, F. Meng, C. Ding, P. K. Chu and X. Liu, *Acta Biomater.*, 2010, **6**, 990.
16. G. Wang, Z. Lu, X. Liu, X. Zhou, C. Ding and H. Zreiqat, *J. R. Soc. Interface*, 2011, **8** 1192.
17. G. Wang, Z. Lu, D. Dwarte and H. Zreiqat, *Mater. Sci. Eng. C*, 2012, **32**, 1818.
18. G. Wang, Z. Lu, K. Y. Xie, W. Y. Lu, S. I. Roohani-Esfahani, A. Kondyurin and H. Zreiqat, *J. Mater. Chem.*, 2012, **22**, 19081.
19. G. Wang, X. Liu, J. Gao and C. Ding, *Acta Biomater.*, 2009, **5**, 2270.
20. C. W. Kang and H. W. Ng, *Surf. Coat. Technol.*, 2006, **200**, 5462.
21. G. Wang, X. Liu, H. Zreiqat and C. Ding, *Colloids Surf. B*, 2011, **86**, 267.
22. R. G. Flemming, C. J. Murphy, G. A. Abrams, S. L. Goodman and P. F. Nealey, *Biomaterials*, 1999, **20**, 573.
23. M. Lampin, R. Warocquier-Clerout, C. Legris, M. Degrange and M. F. Sigot-Luizard, *J. Biomed. Mater. Res.*, 1997, **36**, 99.
24. E. Eisenbarth, D. Velten, M. Müller, R. Thull and J. Breme, *J. Biomed. Mater. Res. A*, 2006, **79**, 166.
25. K. A. Michalow, D. Flak, A. Heel, M. Parlinska-Wojtan, M. Rekas and T. Graule, *Environ. Sci. Pollut. Res.*, 2012, **19**, 3696.
26. C. Liu, L. Miao, J. Zhou, R. Huang and S. Tanemura, *J. Mater. Chem.*, 2012, **22**, 14180.
27. M. Hirano and Y. Ichihashi, *J. Mater. Sci.*, 2009, **44**, 6135.
28. J. Arbiol, J. Cerdà, G. Dezanneau, A. Cirera, F. Peiró, A. Cornet and J. R. Morante, *J. Appl. Phys.*, 2002, **92**, 853.
29. F. I. Trifa, G. Montavon, C. Coddet, P. Nardin and M. Abrudeanu, *Mater. Charact.*, 2005, **54**, 157.
30. S. Sampath and H. Herman, *J. Therm. Spray Technol.*, 1996, **5**, 445.
31. Y. C. Yang and B. Y. Chou, *Mater. Chem. Phys.*, 2007, **104**, 312.
32. W. Q. Yan, T. Nakamura, K. Kawanabe, S. Nishigochi, M. Oka and T. Kokubo, *Biomaterials*, 1997, **18**, 1185.
33. S. P. Singh, K. Pal, A. Tarafder, M. Das, K. Annapurna and B. Karmakar, *Bull. Mater. Sci.*, 2010, **33**, 33.
34. W. R. Manning, O. Hunter JR, F. W. Calderwood and D. W. Stacy, *J. Am. Ceram. Soc.*, 1972, **55**, 342.
35. S. Zinelis, A. Tsetsekou and T. Papadopoulos, *J. Prosthet. Dent.*, 2003, **90**, 332.
36. R. Karpagavalli, A. Zhou, P. Chellamuthu and K. Nguyen, *J. Biomed. Mater. Res. A*, 2007, **83**, 1087.
37. P. M. Natishan, E. McCafferty and G. K. Hubler, *J. Electrochem. Soc.*, 1988, **135**, 321.
38. M. Kosmulski, *J. Colloid Interf. Sci.*, 2006, **298**, 730.
39. D. Ding, C. Ning, L. Huang, F. Jin, Y. Hao, S. Bai, Y. Li, M. Li and D. Mao, *Nanotechnology*, 2009, **20**, 305103.
40. G. Mendonca, D. B. S. Mendonca, F. J. L. Aragão and L. F. Cooper, *Biomaterials*, 2008, **29**, 3822.
41. T. Amna, M. S. Hassan, W. S. Shin, H. V. Ba, H. K. Lee, M. S. Khil and I. H. Hwang, *Colloids Surf. B*, 2013, **101**, 424.
42. L. Zhao, L. Liu, Z. Wu, Y. Zhang and P. K. Chu, *Biomaterials*, 2012, **33**, 2629.
43. C. Y. Chiang, S. H. Chiou, W. E. Yang, M. L. Hsu, M. C. Yung, M. L. Tsai, L. K. Chen and H. H. Huang, *Dent. Mater.*, 2009, **25**, 1022.
44. S. I. Roohani-Esfahani, S. Nouri-Khorasani, Z. Lu, R. Appleyard and H. Zreiqat, *Biomaterials*, 2010, **31**, 5498.

